

A Novel Method for the Location of High Impedance Faults

Suiksha Gautam

Thesis submitted to the Faculty of the
Virginia Polytechnic Institute and State University
in partial fulfillment of the requirements for the degree of

Master of science
in
Electrical Engineering

Virgilio Centeno, Chair
Chen-Ching Liu
Vassilis Kekatos

May 6, 2024
Blacksburg, Virginia

Keywords: HIF, Harmonics, Mutual Impedance, etc.

A Novel Method for the Location of High Impedance Faults

Suiksha Gautam

(ABSTRACT)

In order to maintain the system reliability and minimize the impact of faults in a distribution system, a timely restoration is needed which requires accurate fault localization. Locating High Impedance Faults (HIFs) is specifically challenging because of their variable and non-linear nature. Most existing approaches focus on identifying the accurate fault distance occurring in the main trunk of a system, often leaving lateral branches as blind spots. To find the accurate distance to the fault in a lateral branches, a single ended fault location algorithm is proposed that uses synchronized voltage and current measurements from PMUs positioned along the trunk. Initially, a specific model that incorporates the particular characteristics of the fault is developed in the spectral domain. Subsequently, a fault location algorithm is developed that utilizes the change in a voltage of a healthy phase for calculating the accurate distance to the fault. Extensive simulations performed across different systems at different conditions prove the efficacy of the algorithm. Notably, a critical prerequisite for the algorithm's success is the presence of at least one healthy phase running parallel to the faulty phase.

A Novel Method for the Location of High Impedance Faults

Suiksha Gautam

(GENERAL AUDIENCE ABSTRACT)

High Impedance Faults (HIFs) in power systems often involve dangerous arcing, posing significant risks to life and property. Accurate fault location is essential to ensure timely restoration of power and mitigate hazards. While existing literature typically focuses on the location of faults in the main trunk lines, distribution systems with numerous lateral branches require precise fault distance determination in these branches for faster restoration. This study introduces a novel approach leveraging Phasor Measurement Units (PMUs) in main feeders to pinpoint fault distances in lateral branches. By analyzing voltage variations in healthy phases, the algorithm accurately determines the distance to the fault in the affected phase. Extensive testing across various systems demonstrates the algorithm's high accuracy. The presence of a healthy phase parallel to the faulty phase is essential for the working of this algorithm. This approach offers a promising solution for enhancing the accuracy of fault location in distribution systems, thereby improving outage response times.

Dedication

To my Parents

Acknowledgments

I would like to express my sincere gratitude to my advisor, Dr. Virgilio Centeno for his constant motivation and guidance throughout my research work. His encouragement has not only shaped my academic endeavors but has also instilled in me invaluable skills and confidence to navigate challenges and strive for excellence in my research pursuits.

I extend heartfelt gratitude to Dr. Chen Ching Liu and Dr. Vassilis Kekatos for their invaluable contributions to my academic journey. Their mentorship, expertise, and commitment to cultivating a supportive environment within the Power and Energy Center (PEC) group have profoundly impacted my academic and personal development.

I also wish to express my sincere appreciation to Dr. Maicon Ramos for his patience, guidance, and willingness to address my inquiries. Furthermore, I extend my gratitude to my colleagues Imtiaj, Vishal, Ashutossh, Francisco and Yi jie for their camaraderie and assistance during our shared experiences in Whittemore 422 and 419.

To my dear friends in Blacksburg, Narayan, Sophiya, Arati, and Prakash, you have been like a family to me, and I am deeply grateful for your unwavering support, encouragement, and companionship throughout my journey. Your presence has been a source of joy and strength during both challenging and joyous times.

Finally, I am immensely grateful to my family for their unwavering support, boundless love, and selfless sacrifices. Their belief in my aspirations has propelled me forward, motivating

me to overcome every obstacle and enriching my life in ways beyond measure.

Contents

- List of Figures ix

- List of Tables xi

- 1 Introduction 1**
 - 1.1 Prior Work 2
 - 1.2 Objective and Contribution 6
 - 1.3 Thesis Outline 7

- 2 Phasor Estimation and Fault Model 8**
 - 2.1 Phasor Estimation 8
 - 2.1.1 Fundamentals of Phasor Representation 9
 - 2.1.2 DFT and Fourier Series 9
 - 2.1.3 Phasor representation using Fourier Series 10
 - 2.2 Spectral Leakage Phenomenon 11
 - 2.3 Distribution System Line Model 14
 - 2.4 Load Model 17
 - 2.5 High Impedance Fault Model 17

3	Fault Location Algorithms	22
3.1	Fault location using two end synchronized harmonic measurements	23
3.2	Problem with Single Ended Fault Location Algorithm	25
3.3	A Novel Single Ended Fault Location Algorithm	26
3.3.1	Estimation of Load Current in the faulted Phase	29
3.3.2	A single lateral case	30
3.3.3	Two lateral case	31
4	Result	33
4.1	A single lateral Case	33
4.2	Two lateral Case	36
4.3	Six Bus System	38
4.4	Comparison of different windows for phasor computation	41
4.5	Sensitivity Analysis	42
4.5.1	Sensitivity to noise	42
4.5.2	Sensitivity to load	42
5	Conclusions and Future Work	44

List of Figures

2.1	Windows analyzed for DFT computation	13
2.2	Three phase line segment Model(Adapted from [21])	15
2.3	Characteristics of fault current during HIF	18
2.4	Emanuel Model	19
2.5	HIF as two series connected TVRs	20
2.6	Presence of higher order component in HIF	21
3.1	A flowchart describing the fault location methodology	22
3.2	A radial system	23
3.3	HIF as third harmonic current source	24
3.4	HIF at Phase C	25
3.5	System with a single lateral	30
3.6	System with two laterals	31
4.1	Faults at different phases	35
4.2	Faults at different phases	37
4.3	Six Bus System [15]	38
4.4	Fault at phase A in 2nd lateral	41

4.5	Estimated distance percentage error as a function of distance considering noise in the measurement	43
4.6	Estimated distance percentage error as a function of distance under different load conditions	43

List of Tables

2.1	Parameters of Blackman-Harris family (Adpated from [20])	14
4.1	Comparison of Expected and Calculated Fault Distances	34
4.2	Comparison of Expected and Calculated Fault Distances	36
4.3	Percentage error in fault distance calculation using two-ended FLA	39
4.4	Calculated distance to the fault using single-ended FLA	40

Chapter 1

Introduction

The reliability, safety and power quality of electrical supply is a great concern for industrial, commercial and residential customers given the facets of modern lives depend on uninterrupted electricity. Unlike their transmission counterparts, distribution networks are recognized for their complex structure, featuring branches and tapped laterals that enable the distribution of electricity to end-users. These networks extend across both rural and urban areas, facing susceptibility to numerous fault sources, including adverse weather conditions, bird contacts, vegetation growth, and equipment failures [1]. Around 5-20% of faults in distribution systems are attributed to High Impedance Faults (HIFs), representing only instances where these HIFs subsequently escalated into high-current short circuits[2]. A HIF occurs when an energized conductor establishes poor contact with the ground or interferes with the quasi insulating object such as tree,poles or other equipment [3]. In underground system, they occur due to insulation degradation that exposes the energized conductor to high impedance objects. HIF is characterized by low intensity of fault current and non-significant change in the voltage which poses challenge for both the detection and the location of the fault. Most notably, these faults accompany arcing phenomena which can lead to fire, introducing a potential hazard to public safety. In some instances when HIFs results in conductor rupture, it can lead to the interruption of electricity [4]. The nonlinearity of arc resistance and the relative low magnitudes of fault currents associated with HIFs create hurdles for its precise detection and location[5].

HIF is notably less common in transmission and subtransmission system, one reason being the design of transmission system. As there is carefully planned clearance, the probability of downed conductor or contact with the tree limb is much lower. Even if these faults occur, the short circuit power in transmission system is higher and the currents to the ground can be detected more easily. Despite the extended tripping times and unselective trips associated with HIF in transmission systems, these faults seldom go unnoticed due to the heightened sensitivity of detection mechanisms. But, in distribution system there are various challenges that are introduced by HIFs. The exploration of research pertaining to this fault category began in 1970s [6]. Since, then subsequent research has focused on fault detection[7], [8]. However, the establishment of a comprehensive protective framework should encompass fault localization, with the objective of minimizing the duration required for utility maintenance teams to pinpoint the fault location and expedite the restoration of energy supply.[5].

1.1 Prior Work

For the location of high impedance fault time-domain, frequency-domain, and time-frequency domain methods, have been studied. In [9], the authors have used time-domain approach to estimate the fault distance and fault parameters using parameter estimation approach. Emanuel model [10] is used for modeling HIF and involves resistance and inductance, with positive and negative arc voltages switched based on the signal semi-cycle. The linear least square estimation (LSE) method is utilized for estimating unknown parameters when line capacitors are not considered in the equations. In scenarios involving capacitors, a nonlinear least square estimation approach (NLLSE) is adopted, employing Newton's method with steepest descent to accommodate the non-linear relationship in parameter estimation. The NLLSE is used to refine the estimates obtained from the linear LSE method. The method

is interesting but the location of the fault has been only evaluated in the trunk and the fault in the branches hasn't been studied. The utilization of a time-domain system may exhibit certain constraints in contrast to frequency domain approaches, including the presence of noise in the signal, harmonic distortion, and inherent challenges in implementation[11]. Thus, the author of [12], [13] propose a frequency domain method using impedance based approach for HIF location with measurement only at one end. In [12], the authors have used the fundamental frequency component for location of the fault. Due to the non-linear nature of the fault, the resulting equation becomes underdetermined with three unknowns and two equations. A moving time window approach is been proposed in [12] to convert it into an overdetermined equation. By applying Fourier transform to a moving window, the resulting equations become overdetermined, leveraging the constant magnitude and rotating phasor concept. WLS minimization is achieved through the Newton-Raphson method, with higher weight assigned to recently obtained samples. Fault current is initially calculated as the difference between pre-fault and post-fault current, and is refined iteratively until a specified tolerance is met. Given the considerable variation of fault parameters during HIF, residual-based method using a Binary Control Variable (BCV) is used for precise estimate selection in the Weighted Least Squares (WLS) approach. Residuals exceeding 3 Standard Deviations (SD) are ignored, setting BCV to zero. If below 3 SD, BCV is 1, indicating selection. The proposed approach has been verified in IEEE 13 system model and a real distribution system from the RGE SulPower Utility (Southern Brazil) with a very good accuracy. According to the author of [13], employing a mathematical model that exclusively consider fundamental components results in an overdetermined system of algebraic linear equations characterized by a high degree of linear dependence. This can result in a parameter matrix that approaches singularity, leading to solutions characterized by substantial estimation errors. So, in [13], the author has used third harmonic component in addition to the fundamental to make the system determined. A Parametric Error Processing (PEP) method, leveraging Composed

Measurement Error Normalized (CMEN), is proposed for identifying and rectifying errors in parameters associated with HIF current distortions. In the proposed method, sensitivity analysis revealed the method's robustness in fault distance estimation under varying fault parameters (arc voltage amplitude, fault resistance) and system load conditions. This method has contributed a robust and effective analytical formulation for high impedance fault location, offering improvements over existing techniques. However, the possibility of multiple estimation problem in the presence of laterals hasn't been explored and like any other single ended impedance based method, it also faces multiple estimation problem.

In [14], the author introduces a two-ended impedance-based method for fault detection and localization in transmission lines. The method is fault-type independent and utilizes a least squares algorithm for accurate fault distance estimation. The proposed approach is applicable to single line to ground faults, double line to ground faults and both low and high impedance faults. As, this method doesn't depend on the model of the fault, similar approach is used for both low and high impedance fault. The incorporation of the least squares approach addresses noise and unmodeled effects, enhancing the accuracy of fault distance calculations minimizing estimation errors. Through sensitivity analysis using analysis of variance (ANOVA), the study identifies the distance of the fault, error in line parameters, and noise in the signal as significant factors. Conversely, the nature of the fault, fault resistance, and angle of incidence prove to be insignificant for the proposed method. The approach achieves a commendable maximum error of 0.25%, with 80% of cases demonstrating an error below 0.015%. Authors have claimed that the method has the potential for real-life applications. However, the use of a Digital Fault Recorder (DFR) at every node of the power system makes this method economically infeasible. Similarly, the study of [15] introduces a two-ended impedance-based method utilizing zero-sequence voltage and sequence current for locating High Impedance Faults (HIFs). It uses Fortescue theorem to convert

phase impedance, voltage and current to sequence terms in both balanced and unbalanced distribution system. It emphasizes the variation of induced voltage drop ($\Delta V_0, t$) in the zero-sequence, highlighting its non-uniformity across different sections. This variability is closely associated with the positive sequence current drawn by individual transformers (denoted as $I_{t,n}$ and $I_{r,m}$, where 'n' and 'm' represent the number of transformers upstream and downstream from the fault point). To address this, the author in [15] introduce a linear approximation to rectify the induced voltage drop in the zero sequence. This correction aims to improve the accuracy of estimates provided by meters M1 and M2. The correction is done for negative sequence as well. The method is proved to be robust against load variation and the presence of DG in the system. However, in scenarios where the fault occurs in the lateral, the method can identify the lateral branch but lacks precision in determining the exact distance to the fault. Placing an extra PMU in the lateral would give the exact distance to the fault in the lateral.

There are several methods that combine signal processing with machine learning algorithms for the location of the HIF. Signal processing tools are used for generating features for machine learning algorithms. In a recent study [4], the authors have reviewed the existing high impedance fault location approaches and have proposed a new methodology to identify a fault region using random forest algorithm. The main contribution according to the author is to address the lack of consensus on input features, metrics and decision algorithm. Harmonics are extracted using Stockwell transform that is an effective representation of time varying harmonics. Energy of each harmonic at each cycle is computed for the phase and neutral current measured at the substation. To ensure optimal feature selection with minimal redundancy and maximal relevance, the minimal redundancy maximal relevance (mRMR) approach is employed. And, the random forest algorithm is chosen to output the faulted section due to its better accuracy. The method has good accuracy even in the presence of

noise. However, the Stockwell transform algorithm is computationally expensive and can hinder real time location of faults. Also, the performance of the algorithm heavily relies on the quality of the training data. Similarly, the author of [16] uses synchronized phasor measurement unit data as the input of ANN to identify the faulted lateral and the distance to the fault from the first meter in an area. In the first step, the faulted phase and area of the fault is identified and this information is used in the second step to calculate the distance to the fault. The database for training the ANN incorporates various realistic scenarios, including changes in feeder resistance due to temperature variations, load variations, different distribution system topologies, and different positions, sizes and types of Distributed Generation (DG) units, as well as random fault characteristics such as different fault resistances and locations at various phases. Multiple layer feedforward neural network is used with the number of neurons variation from 1 to 50 in the hidden layer. Levenberg-Marquardt method is used for backpropagation. The ANN model is given two extra inputs, sum of zero sequence current to identify phase to ground fault and sum of negative sequence to detect fault. The method has been verified on the IEEE-123 distribution system and a simple 6 bus system with errors less than 1% for fault location. However, machine learning method requires large amount of training data to train a specific system under different scenarios which might not be available in a real case. Similarly, it is highly likely that the model trained for one specific case and system doesn't provide good accuracy for a different system.

1.2 Objective and Contribution

The main focus of this work is to develop a novel method to identify the distance to a HIF in the branches of a distribution system. The following contributions are made in this work:

1. A novel single-ended method using measurements of healthy phases is developed for

calculating the distance to the fault from the measurement point.

2. The spectral leakage phenomenon while calculating phasors during HIF using rectangular window is addressed.
3. Various simulations are conducted under different system conditions to verify the efficacy of the fault location algorithm.

1.3 Thesis Outline

The thesis is organized as follows:

1. Chapter 1 provides an overview of the problem and delves into existing literature, highlighting their contributions while also pinpointing their limitations, which serve as the motivation for this research.
2. Chapter 2 explains how phasors are calculated for this work, spectral leakage phenomenon while using different windows, and explains the HIF and distribution system model.
3. Chapter 3 explains double ended FLA and a novel single ended FLA.
4. Chapter 4 summarizes the results, demonstrating the efficacy of the algorithm across various scenarios.
5. Chapter 5 discusses the conclusion and outlines future direction of the work.

Chapter 2

Phasor Estimation and Fault Model

This chapter delves into Phasor estimation algorithm, spectral leakage phenomenon in phasor computation and also describes the HIF model and exact distribution system model. These models provide the framework for the work presented in this thesis.

2.1 Phasor Estimation

Measuring angles between distant point had been a great concern in power system. With the advent of GPS technology, measurements can be referenced to the GPS time, synchronizing devices across the grid. Standing at the forefront of this transformation are Phasor Measurement Units (PMUs), adept at capturing real-time measurements of current, voltage, and phase angles, time synchronized with high GPS precision. This extensive dataset, gathered from multiple grid locations, significantly improves reliability and operational efficiency. Various applications for PMUs have emerged, notably in fault location, where precise timing and synchronization capabilities are important.

2.1.1 Fundamentals of Phasor Representation

A pure sinusoidal signal can be represented as:

$$x(t) = X_m \cos(\omega t + \phi) \quad (2.1)$$

where X_m is the peak amplitude of the signal and ω is the frequency of the signal in radians per second. In phasor form, it can be represented as:

$$X = \left(\frac{X_m}{\sqrt{2}} \right) [\cos \phi + j \sin \phi] \quad (2.2)$$

where $\frac{X_m}{\sqrt{2}}$ is the rms magnitude of the signal and ϕ represents the phase angle. In reality, the signal is corrupted with harmonics and noise. To extract the phasor of specific harmonic component of a signal, we need to perform a discrete Fourier transform (DFT) of the sampled signal[17].

2.1.2 DFT and Fourier Series

Taking an input signal $x(t)$ which is being sampled at uniform intervals $k\Delta T$ where ($k = 0, \pm 1, \pm 2, \pm 3, \dots$) and yields sampled data $x(k\Delta T)$. To select N samples to perform DFT, we need to multiply the signal with a windowing function $w(t)$ which has unit magnitude and spans over $N\Delta T$. Within the window, we will have $x(k\Delta T)$ samples. It can be seen as multiplying the signal $x(t)$ with the windowing function $w(t)$ and the sampling function δt .

$$y(t) = x(t)\delta(t)\omega(t) = \sum_{k=0}^{N-1} x(k\Delta t)\delta(t - k\Delta T) \quad (2.3)$$

By taking the convolution of these three signals in the frequency domain, we can calculate the DFT of the signal. The DFT of the signal is given as:

$$X(f) = \sum_{k=0}^{N-1} x(k\Delta T) e^{-j2\pi kn/N} \quad (2.4)$$

The Fourier series coefficients of a periodic signal can be obtained by dividing the DFT result by the sum of the amplitude of all samples of a window. Thus, the Fourier series coefficients for $x(t)$ are given by:

$$x(t) = \sum_{k=-\infty}^{\infty} \alpha_k e^{j2\pi kt/T} = \sum_{k=-\infty}^{\infty} \left[\frac{1}{N} \sum_{n=0}^{N-1} x(k\Delta T) e^{-j2\pi kn/N} \right] e^{j2\pi kt/T} \quad (2.5)$$

Using the Fourier coefficients on sampled data, we can determine phasors for any harmonic.

2.1.3 Phasor representation using Fourier Series

Consider a sinusoidal function $x(t)$ with frequency kf_0 expressed as:

$$x(t) = a_k \cos(2\pi k f_0 t) + b_k \sin(2\pi k f_0 t) = \sqrt{(a_k^2 + b_k^2)} \cos(2\pi k f_0 t + \phi)$$

where $\phi = \tan^{-1} \left(\frac{-b_k}{a_k} \right)$.

The phasor representation X_k of $x(t)$ is given by:

$$X_k = \sqrt{a_k^2 + b_k^2} e^{j\phi} = (a_k - jb_k)$$

The estimated value of the k th harmonic component, X_k , using N samples per cycle is computed using the relationship of DFT with fourier series as:

$$X_k = \frac{2}{N} \sum_{n=0}^{N-1} x(n\Delta T) (\cos(kn\theta) - j \sin(kn\theta))$$

where,

$\theta = \frac{2\pi}{N}$ and N is the sum of the coefficients of a window

k is the harmonic number and 0 is for dc component, 1 is for fundamental and so on.

n is the sample number in a cycle.

It can be represented in matrix form as:

$$\begin{bmatrix} X(0) \\ X(1) \\ \vdots \\ X(k) \end{bmatrix} = \frac{2}{N} \begin{bmatrix} (C_w - jS_w)_{(0,0)} & (C_w - jS_w)_{(0,1)} & \dots & (C_w - jS_w)_{(0,N-1)} \\ (C_w - jS_w)_{(1,0)} & (C_w - jS_w)_{(1,1)} & \dots & (C_w - jS_w)_{(1,N-1)} \\ \vdots & \vdots & \ddots & \vdots \\ (C_w - jS_w)_{(K,0)} & (C_w - jS_w)_{(K,1)} & \dots & (C_w - jS_w)_{(K,N-1)} \end{bmatrix} * \begin{bmatrix} x(1) \\ x(2) \\ \vdots \\ x(N) \end{bmatrix} \quad (2.6)$$

where, $C_w = \cos \frac{2\pi}{N} kn$ $S_w = \sin \frac{2\pi}{N} kn$

2.2 Spectral Leakage Phenomenon

To extract magnitude and phasor information from a specific segment of a signal using the Discrete Fourier Transform (DFT), applying windows is essential. The rationale behind employing the window is to generate a periodic function capable of replicating the original signal's samples within recurring windows [17]. The abrupt transition from non-zero to zero values at the window edges especially for rectangular windows introduces high-frequency components that spread across the entire frequency domain, causing spectral distortion. Let's assume that the signal is $x(t)$ with a sampling frequency, $f_s = \frac{1}{\Delta t}$, where f_s meets the Nyquist criteria of being more than twice the maximum frequency present in the signal.

Suppose the signal is comprised of a single frequency component.

$$x(t) = A_m e^{j\omega_m t}$$

And the rectangular window is given as:

$$W_T(t) = \begin{cases} 1 & \text{if } 0 < t \leq T \\ 0 & \text{otherwise} \end{cases}$$

The signal with a duration T is given by the product of original signal with the window function

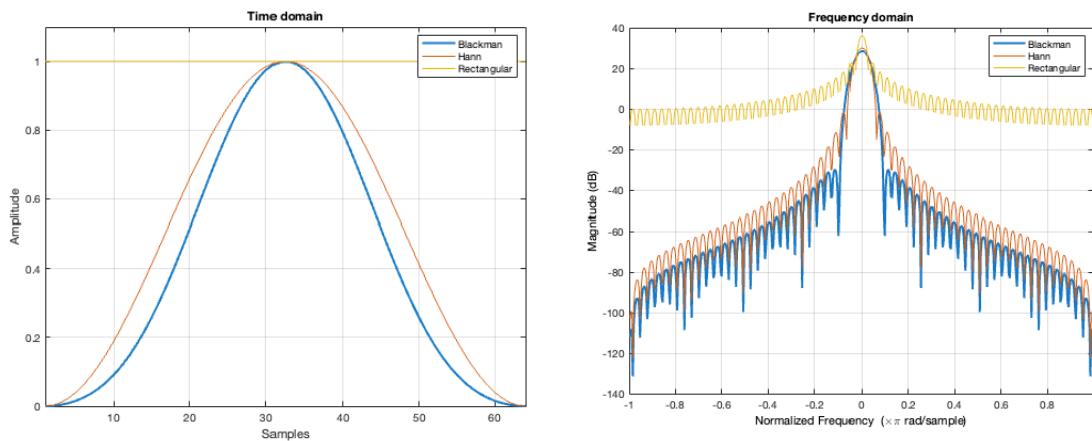
$$x_T(t) = x(t) * W_T(t)$$

The Fourier transform of $x(t)$ is $X_m(\omega) = A_m \cdot 2\pi\delta_{\omega_m}(\omega)$ and yields a single spectrum line, indicative of a concentrated frequency component at ω_0 . And the fourier transform of the rectangular window is given as[18]:

$$W_T(\omega) = \frac{\sin\left(\frac{\omega T}{2}\right)}{\frac{\omega}{2}} e^{-j\left(\frac{\omega T}{2}\right)}$$

In accordance with the Fourier transform product theorem, the convolution of $X_m(\omega)$ and $W_T(\omega)$ gives rise to the Fourier transform of $x_T(t)$. The fourier transform of rectangular window represented in figure 2.1b is characterized by a narrow main lobe and wide side lobes, exhibiting a small ratio between the main lobe and side lobes. This leads to significant "leakage" of side lobes[19]. Leakage signifies that the energy associated with a specific

frequency component spills into neighboring frequencies, leading to potential interference and distortion in the analyzed signal. So, the spectrum of $X_m(\omega)$ is no longer a single line and spreads across the entire frequency range. When there are more side lobes present alongside the main lobe, it leads to a decrease in the magnitude of the main lobe due to leakage. The implications are more profound in the context of harmonic analysis. As energy leaks from various harmonics, it introduces the risk of overlapping spectral components, complicating the accurate identification and analysis of individual harmonic frequencies. This phenomenon may lead to errors in the interpretation of harmonic content, affecting the precision of harmonic analysis techniques. The errors produced by harmonic leakage can be reduced by proper windowing of the signal.



(a) Different windows in time domain (b) Different windows in frequency domain

Figure 2.1: Windows analyzed for DFT computation

Spectral leakage is one of the reason some PMUs like the one developed by Arbiter Systems provide a user selectable wide range of window functions [20]. The Hann (or Hanning) and Blackman windows are often used because their side lobes exhibit a decrease in magnitude as the frequency increases. The Hann, Hamming (2-term), Blackman (3-term), and Nutall (4-term) windows share a common general equations and collectively belong to the Blackman-

Harris family[20]. The general expression of Blackman-Harris family of windows is:

$$w_m(n) = \sum_{m=0}^M (-1)^m a_m \cos\left(\frac{2\pi}{N} mn\right)$$

where M is the number of items minus 1.

Window	a_0	a_1	a_2	a_3
Hann	0.5	0.5	–	–
Hamming	0.54	0.46	–	–
Blackman	0.42	0.5	0.08	–
Nutall	0.355768	0.487396	0.144232	0.012604
Flat-top	0.2810639	0.5208972	0.1980399	–

Table 2.1: Parameters of Blackman-Harris family (Adpated from [20])

The time domain and frequency domain representation of different windows used for comparison in this thesis are shown in 2.1. It is evident that as the value of M increases, the side lobe attenuates greatly reducing the spectral leakage[18]. However, the central lobe expands with increase in M making it more challenging to distinguish between closely spaced frequency components in the signal. This wider central lobe can lead to increased interference between adjacent frequency components, reducing the accuracy of spectral analysis.

2.3 Distribution System Line Model

For precise estimation of voltage and current at specific nodes of a distribution system, an exact line model of the distribution system can be used, facilitating reliable calculations based on measurements from nearby nodes. If we apply Kirchhoff's Current law at node q

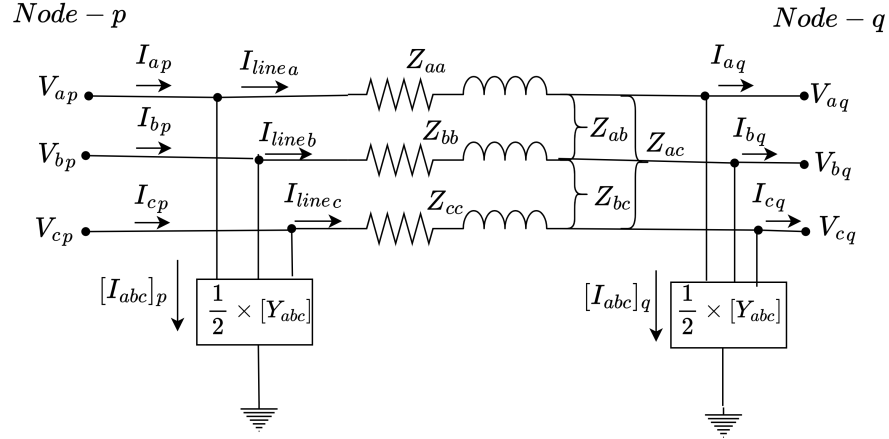


Figure 2.2: Three phase line segment Model(Adapted from [21])

in figure 3.1, we obtain:

$$[I_{line_{abc}}]_q = [I_{abc}]_q + \frac{1}{2} * [Y_{abc}] * [V_{abc}]_q \quad (2.7)$$

Applying Kirchhoff's voltage law at node p, we have:

$$[V_{abc}]_p = [V_{abc}]_q + [Z_{abc}] * [I_{line_{abc}}]_q \quad (2.8)$$

Combining equation 2.7 and 2.8, we obtain a general equation represented as:

$$[V_{abc}]_p = [a] * [V_{abc}]_q + [b] * [I_{abc}]_q \quad (2.9)$$

where,

$$[a] = [u] + \frac{1}{2} * [Z_{abc}] \cdot [Y_{abc}]$$

$$[b] = [Z_{abc}]$$

$[u]$ is a 3×3 identity matrix

Similarly, applying Kirchhoff's current law at node P, we have,

$$[I_{abc}]_p = [Iline_{abc}]_q + \frac{1}{2} * [Y_{abc}] * [V_{abc}]_p \quad (2.10)$$

Combining equation 2.7, 2.8 and 2.10, we obtain an equation whose general representation is given as:

$$[I_{abc}]_p = [c][V_{abc}]_q + [d][I_{abc}]_q \quad (2.11)$$

where,

$$\begin{aligned} [c] &= [Y_{abc}] + \frac{1}{4}[Y_{abc}] \cdot [Z_{abc}] \cdot [Y_{abc}] \\ [d] &= [U] + \frac{1}{2}[Y_{abc}] \cdot [Z_{abc}] = [a] \end{aligned}$$

Equations 2.9 and 2.11 can be written in combined form as:

$$\begin{bmatrix} [V_{abc}]_p \\ [I_{abc}]_p \end{bmatrix}_{6 \times 1} = \begin{bmatrix} [a] & [b] \\ [c] & [d] \end{bmatrix}_{6 \times 6} \cdot \begin{bmatrix} [V_{abc}]_q \\ [I_{abc}]_q \end{bmatrix}_{6 \times 1} \quad (2.12)$$

To solve for voltage and current at node q when these values are given at node p, we use:

$$\begin{bmatrix} [V_{abc}]_q \\ [I_{abc}]_q \end{bmatrix}_{6 \times 1} = \begin{bmatrix} [a] & [b] \\ [c] & [d] \end{bmatrix}_{6 \times 6}^{-1} \cdot \begin{bmatrix} [V_{abc}]_p \\ [I_{abc}]_p \end{bmatrix}_{6 \times 1} \quad (2.13)$$

2.4 Load Model

The load is modeled as a constant impedance because this is the most common model found in recent literature [12], [13] in HIF location and its impedance is given as:

$$\begin{bmatrix} \frac{V_{an}^2}{P_{an}-jQ_{an}} & 0 & 0 \\ 0 & \frac{V_{bn}^2}{P_{bn}-jQ_{bn}} & 0 \\ 0 & 0 & \frac{V_{cn}^2}{P_{cn}-jQ_{cn}} \end{bmatrix} \quad (2.14)$$

where V, P and Q denotes the nominal voltage and active and reactive power respectively.

2.5 High Impedance Fault Model

The impedance of the HIF is dependent on the resistivity of the soil, its moisture content and the composition. In the test conducted in [22], the initial current is only 60% of the full value of the fault current due to smaller effective contact between the conductor and the soil, growing to full value in about three to four cycles. Due to smaller contact area, the density of the current will be large and so the voltage gradient which leads to localized arcing and ionization. Within three to four cycles, the current increases to its full value as the arc penetrates the ground between soil particles, increasing effective contact resistance. As the arc penetrates into the soil, moisture in the vicinity of the arc may be depleted, potentially extinguishing the arc. However, this process is counteracted by the migration of moisture from neighboring soil areas, which can reignite the arc. This phenomenon occurs during the early stage of the failure and is known as intermittency. In contrast to the arcing fault in transmission system that typically exhibit longer arc lengths, higher currents, predominantly inductive impedance, and a uniform contact surface, HIFs are characterized

by shorter arc lengths, lower currents, predominantly resistive impedance, and a non-uniform contact surface due to varying resistivity across soil layers [23]. According to [10], [22], a HIF has the distinct characteristics outlined below and represented in figure 2.3:

1. Non linearity between Voltage and Current due to the presence of electric arc
2. Build up period: During this period, the fault current's amplitude steadily increases
3. Shoulder period: This period marks the stabilization of the fault current's amplitude, occurring after several cycles of current escalation within the buildup period.
4. Asymmetry: There is asymmetry between fault current cycles i.e. the amplitude of positive cycle may become different than that of negative cycle.

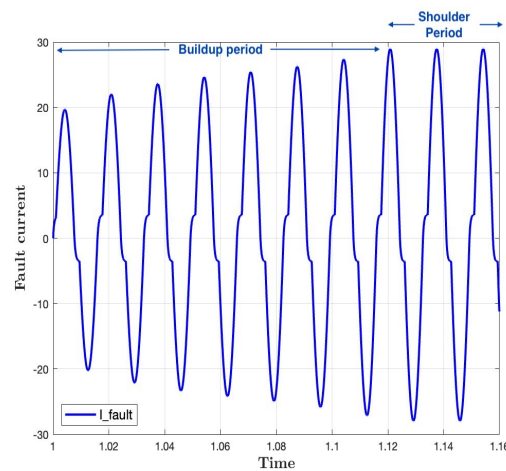


Figure 2.3: Characteristics of fault current during HIF

As cited in [10], the amplitude of the positive half-wave of the fault current exceeds that of the negative half-wave. The discrepancy in amplitude between the positive and negative half-waves of the fault current is not influenced by factors such as electrode shape or the material composition of the electric conductor (e.g., copper or aluminum). Instead, it is dependent upon the moisture content and porosity of the surface in contact. When the surface

experiences heating from a High Impedance Fault (HIF), the silica present in the soil acts as a cathode, emitting electrons. This phenomenon results in smaller voltage drops when the conductor is exposed to positive voltage, as outlined in [23].

Due to the risk and difficulty of obtaining oscillographic records through field test, simulation is the best option to test algorithms for either detecting or locating the HIF. For simulation purpose, in order to build a realistic model of HIF, these stochastic properties have to be accounted in the model. There are many methods to represent HIF in the literature, each aiming to capture the characteristics of HIF.

One notable model is the Emanuel model[10]. It consists of two diodes D_P and D_N , each connected to dc sources and arranged in an anti-parallel manner. The magnitude of dc sources are unequal to model the asymmetry of HIF. The diode and voltage source arrangement are connected in series to the fault resistance and inductance. The value of V_P and V_N depends on the system where the simulation is to be performed and the particular asymmetry under consideration.

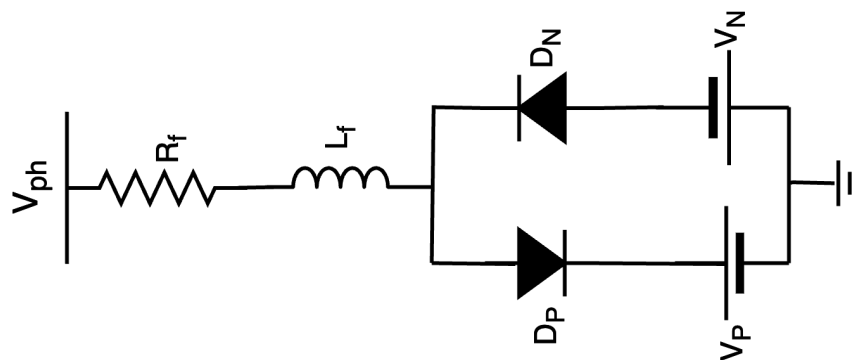


Figure 2.4: Emanuel Model

When the value of $V_{ph} > V_P$, current flows towards the ground and when $V_{ph} < V_N$, the direction of current reverses. When the value of $V_P < V_{ph} < V_N$, no current flows through

the model and this period models the arc phenomenon. Given that the current in the positive half-cycle is greater than in the negative half-cycle, it follows that the voltage across the negative terminal (V_N) is greater than the positive terminal (V_P). This model simulates only the non-linearity and asymmetry characteristics of the fault current.

Another approach to represent the characteristics of HIF is described in [24]. This approach incorporates two resistances connected in series, both of which exhibit time-varying behavior regulated by the Transient Analysis Control System (TACS) module of ATP. The first resistance, denoted as R_1 , is employed to emulate the asymmetry and non-linear properties of the fault. Its value is determined by analyzing the voltage and current during a steady-state period of one cycle. The second resistance, $R_2(t)$, is utilized to model the buildup period (where the current progressively increases) and the subsequent shoulder period (where the current remains constant before increasing again). It is assumed that during steady-state conditions, there is no influence from the buildup and shoulder periods.

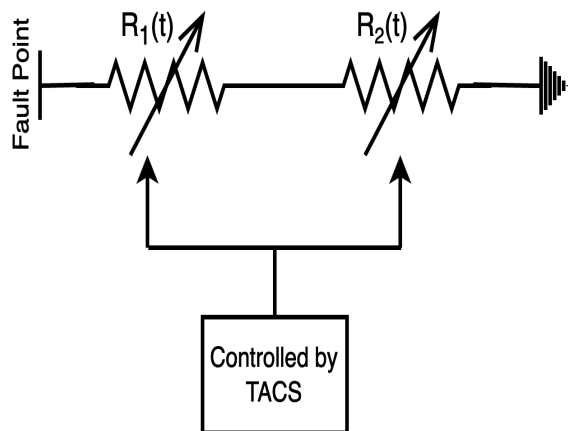


Figure 2.5: HIF as two series connected TVRs

In [23], author presents values of $R_1(t)$ and $R_2(t)$ for simulation of HIF in different types of soils. The time-varying nature of $R_f(t)$ can be divided into two distinct phases: the buildup

period, occurring from t_i to t_{ss} , and the subsequent steady state period beyond t_{ss} . This behavior is approximated by a piecewise polynomial function:

$$R_f(t) = \begin{cases} a_n t^n + a_{n-1} t^{n-1} + \dots + a_1 t + a_0, & \text{for } t_i \leq t \leq t_{ss} \\ a_0, & \text{for } t > t_{ss} \end{cases} \quad (2.15)$$

where, t_i is the instant at which fault occurs and t_{ss} is the instant at which fault reaches a steady state. Equation 2.15 can be used to simulate fault in different soil conditions by varying the coefficients of polynomial. For this thesis work, a modified Emanuel model is used from [14] because of its simplicity to control the percentage of harmonic components generated from the fault. The constant resistance in fig 2.4 is replaced by the time varying resistance represented in equation 2.15. The value of V_P and V_N is used for controlling the percentage of harmonic component and R_f is used for controlling the amplitude of fault current. This model can represent buildup, shoulder, non-linear and asymmetry property of HIF. Among the higher order frequency component, third harmonic component is dominant in HIF followed by fifth harmonic component [25]. The percentage of the magnitude of harmonic components relative to the fundamental component for one of the case in the model is illustrated in figure 2.6.

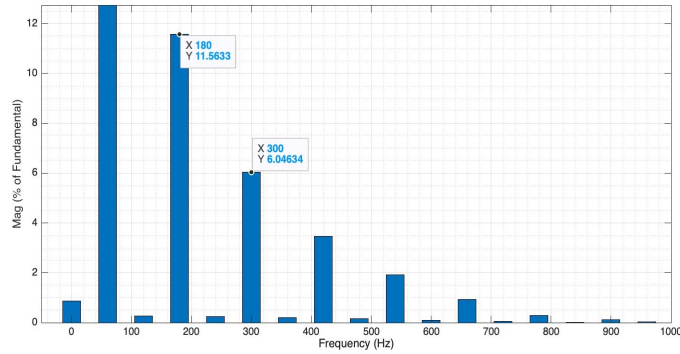


Figure 2.6: Presence of higher order component in HIF

Chapter 3

Fault Location Algorithms

This chapter presents the two ended and a novel single ended fault location algorithm (FLA) designed to determine the distance to a HIF. Firstly, a flowchart is presented explaining the fault location procedure.

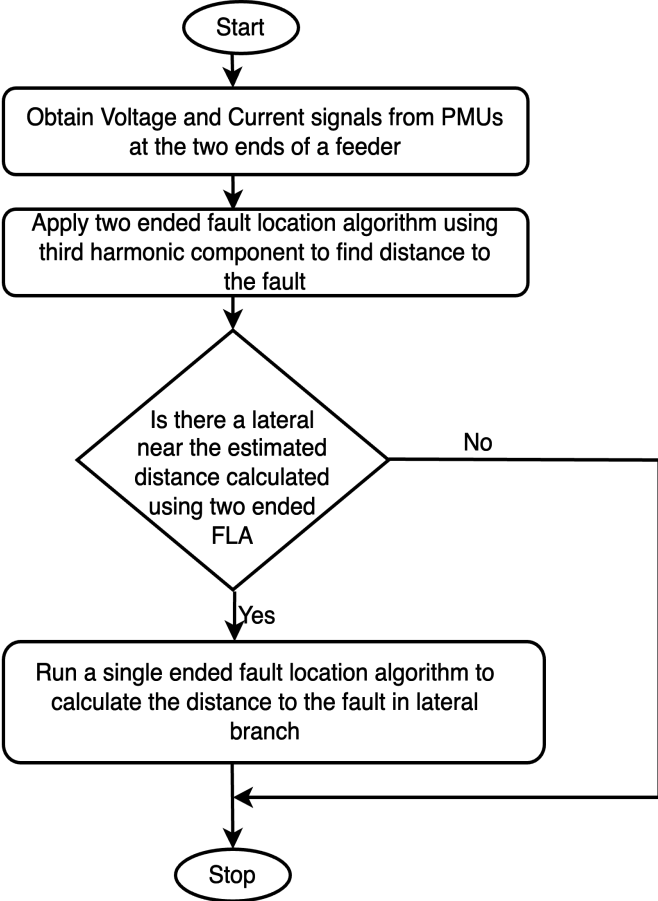


Figure 3.1: A flowchart describing the fault location methodology

3.1 Fault location using two end synchronized harmonic measurements

With the advent of GPS technology, we can get synchronized measurements at different nodes of a power system. Algorithm that uses synchronized voltage and current at two terminals for calculating the accurate distance to the fault are commonly referred as two-ended algorithm. When HIF occurs in a power system, it injects significant third harmonic component into the system. Thus, it can be analyzed as a current source injecting third harmonic current into the system. Most of the harmonic current flows towards the source, this assumption is based on the fact that the impedance to the substations is lower compared to the loads when seen from the fault point[25]. Thus, the current flowing from fault towards the load is negligible compared to the current flowing towards the substation. Consider two PMUs as shown in fig 3.2, where PMU 1 is connected to the node near substation and PMU 2 is connected at the opposite end of a trunk.

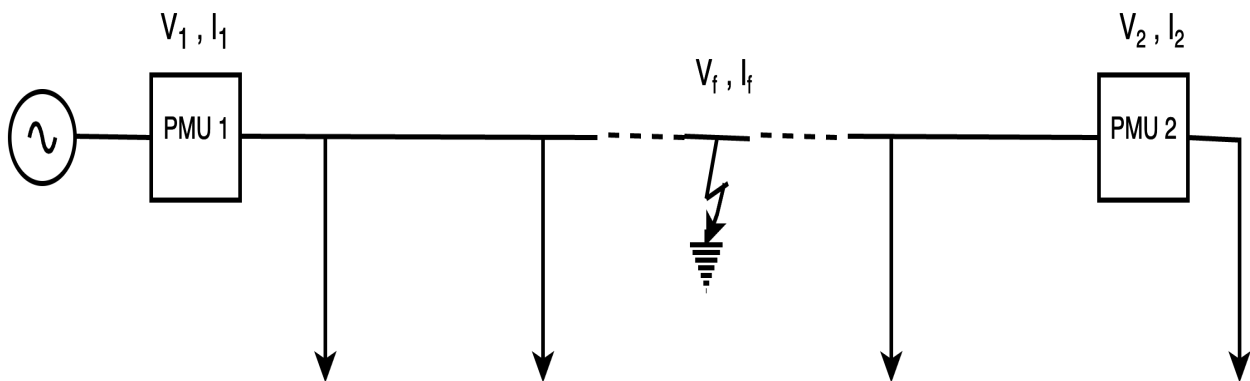


Figure 3.2: A radial system

Suppose the fault occurs at any point 'F' between two PMUs. Considering the current source at point 'F' as shown in figure 3.3, the following relation can be expressed:

$$\begin{aligned} V_f &= V_1 + d_1 \cdot Z_L \cdot I_1 \\ V_f &= V_2 + d_2 \cdot Z_L \cdot I_2 \\ d_1 + d_2 &= 1 \end{aligned} \tag{3.1}$$

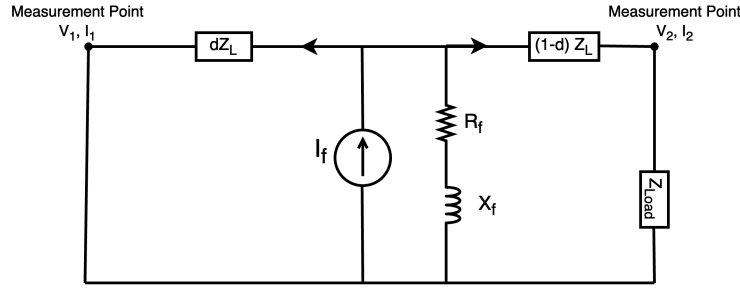


Figure 3.3: HIF as third harmonic current source

where V_1 and I_1 are the third-harmonic voltages and currents measured by PMU_1 and V_2 and I_2 are the third-harmonic voltages and currents measured by PMU_2 and d_1 and d_2 is the percentage of a line from PMU_1 and PMU_2 to the fault respectively and V_f is the voltage at the fault point. By solving above equations, we can find the distance to the fault. Given the predominance of the third harmonic current in HIF, third harmonic components of measurements are used for accurate calculation of the distance to the fault.

The error in the distance calculation is due to the fact that some leakage currents will flow through lateral branches between two PMUs. In scenarios, where there are multiple branches or tapped loads, the error in the calculation of distance goes on increasing, leading to a progressive deviation in the accuracy of fault distance calculation. More PMU can be deployed along the trunk to increase the accuracy. This method is able to calculate the

distance to the fault when the fault occurs in the trunk of a power system. However, when faults occur in any branches, then it is only able to identify the location in the main trunk where the lateral is connected. This highlights the challenge of observing laterals through PMUs placed at trunk's ends. Placing an extra PMU at the end of the lateral can make the lateral observable. However, distribution system have multiple lateral branches and PMUs in distribution are still scarce. The combination of two end synchronized fault location algorithm and a single ended fault location algorithm using fundamental component can be used for finding the accurate distance to the fault in the lateral branch.

3.2 Problem with Single Ended Fault Location Algorithm

Let's consider a case with a HIF at phase C at $d\%$ of the line in a lateral. The phase C with a HIF is represented in figure 3.4

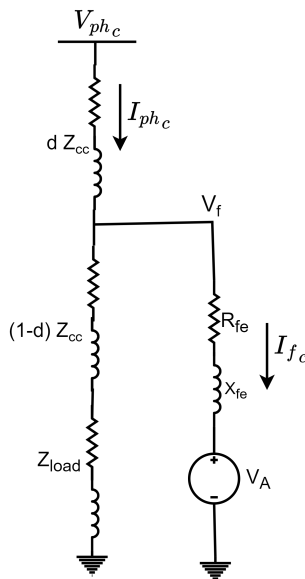


Figure 3.4: HIF at Phase C

The voltage at phase C can be represented as:

$$V_{\text{ph}_c} = d(I_{\text{ph}_a} Z_{ac} + I_{\text{ph}_b} Z_{bc} + I_{\text{ph}_c} Z_{cc}) + V_f \quad (3.2)$$

$$V_{\text{ph}_c} = dM_{\text{ph}_c} + I_{f_c} Z_{fe} \quad (3.3)$$

Where,

$$V_f = I_{f_c} Z_{fe}$$

$$M_{\text{ph}_c} = I_{\text{ph}_a} Z_{ac} + I_{\text{ph}_b} Z_{bc} + I_{\text{ph}_c} Z_{cc}$$

$$Z_{fe} = Z_f + Z_A$$

Z_f and Z_A are the fault and arc impedance respectively.

Separating equation 3.3 into real and imaginary parts, we have,

$$\begin{bmatrix} V_{\text{ph}_c}^r \\ V_{\text{ph}_c}^i \end{bmatrix} = \begin{bmatrix} M_{\text{ph}_c}^r & I_{f_c}^r & -I_{f_c}^i \\ M_{\text{ph}_c}^i & I_{f_c}^i & I_{f_c}^r \end{bmatrix} \cdot \begin{bmatrix} d \\ R_{fe} \\ X_{fe} \end{bmatrix} \quad (3.4)$$

Equation 3.4 has three unknowns and only two equations. So, the equation is underdetermined. Thus, we need to find a new method to find the distance to the fault using measurement at only one end for a HIF.

3.3 A Novel Single Ended Fault Location Algorithm

Algorithms that utilize voltage and current measurements of a single terminal to calculate the distance to a fault are commonly referred to as single-ended algorithms. When the con-

ductors are carrying current in a parallel path, their electromagnetic fields interact with each other, leading to mutual coupling effects. This mutual coupling phenomenon is described by the influence of current flow in one circuit to the voltage profile in the other circuit [26]. Therefore, the voltage profile in a specific circuit is not solely determined by the current flowing through that particular circuit. Instead, it is intricately influenced by the currents in its neighboring lines. In a normal condition, the voltage in three phases can be expressed as:

$$\begin{bmatrix} V_{ag} \\ V_{bg} \\ V_{cg} \end{bmatrix} = \left(\begin{bmatrix} Z_{aa} & Z_{ab} & Z_{ac} \\ Z_{ba} & Z_{bb} & Z_{bc} \\ Z_{ca} & Z_{cb} & Z_{cc} \end{bmatrix} + \begin{bmatrix} Z_{load_a} & 0 & 0 \\ 0 & Z_{load_b} & 0 \\ 0 & 0 & Z_{load_c} \end{bmatrix} \right) \times \begin{bmatrix} I_a \\ I_b \\ I_c \end{bmatrix} \quad (3.5)$$

where,

V_{ag} , V_{bg} , and V_{cg} are the line-to-ground voltages.

I_a , I_b , and I_c are the line currents.

Z_{aa} , Z_{bb} , Z_{cc} represent the self-impedance of different phases, and Z_{ab} , Z_{ac} , Z_{ba} , Z_{bc} , Z_{ca} , Z_{cb} represents the mutual impedance between phases.

Z_{load_a} , Z_{load_b} , and Z_{load_c} denote the load impedances.

When a high impedance fault occurs in any phase, there is typically an observed increase of approximately 10-20% in the current within that specific phase. Assuming all other factors remain constant in a system immediately before and after the fault, this increase in current influences the voltage profile in other phases. So, the change in the voltage in other phases during fault is due to the increment of current in the faulted phase. In [27], a two ended fault location algorithm is proposed to calculate the distance to the fault using mutual impedance for a series compensated line. The Zero sequence and positive sequence

impedance was needed for computing mutual impedance. The computed mutual impedance is directly correlated with the distance separating the relay and the fault point. In order to determine the distance to the fault in a lateral branch using measurements taken at two ends of a trunk, a single-ended fault location algorithm is required. Let us assume that $V_{a_{\text{prefault}}}$, $V_{b_{\text{prefault}}}$, and $V_{c_{\text{prefault}}}$ are the fundamental prefault voltages in phase a,b and c respectively. Similarly, $I_{a_{\text{prefault}}}$, $I_{b_{\text{prefault}}}$, and $I_{c_{\text{prefault}}}$ are the fundamental currents in phase a,b,c respectively. Additionally, V_a, V_b, V_c and I_a, I_b, I_c are the fundamental voltages and currents in phase a,b and c respectively. Considering a fault in phase c at a distance $d\%$ from the measurement point, the change in voltage in phases a and b can be expressed as follows:

$$\begin{aligned} V_a - V_{a_{\text{prefault}}} &= (I_a - I_{a_{\text{prefault}}}) \cdot (Z_{aa} + Z_{\text{loada}}) \\ &+ (I_b - I_{b_{\text{prefault}}}) \cdot Z_{ab} + (I_c - I_{c_{\text{prefault}}}) \cdot d \cdot Z_{ac} \end{aligned} \quad (3.6)$$

$$\begin{aligned} V_b - V_{b_{\text{prefault}}} &= (I_b - I_{b_{\text{prefault}}}) \cdot (Z_{bb} + Z_{\text{loadb}}) \\ &+ (I_a - I_{a_{\text{prefault}}}) \cdot Z_{ba} + (I_c - I_{c_{\text{prefault}}}) \cdot d \cdot Z_{bc} \end{aligned}$$

By solving any of the above two equation, we can find the distance of the fault from the point in the trunk where the lateral is connected. The impedance of loads can be derived from the pre-fault condition utilizing equation 3.5, which establishes the relationship between voltage and current. During High-Impedance Faults (HIF), there's a negligible change in voltage at the fault point. Therefore, the current flowing through the load in the faulted phase is assumed to remain approximately the same as it was four cycles before the fault occurred while deriving equation 3.6. This assumption is the primary cause of the minor error observed in distance calculations in the initial iteration.

3.3.1 Estimation of Load Current in the faulted Phase

Since, the assumption of constant load current in the faulted phase in equation 3.6 introduces a degree of error in the calculation of fault distance, there is an opportunity for refinement. To achieve this precision, it is imperative to account for the variability in the load current in the faulted phase and integrate it into equation 3.6. In refining fault distance calculations, the initial estimate of fault distance for a three-phase system with a single line-to-ground fault is derived from the average distance of the two healthy phases, while for a two-phase system with the same fault, the initial estimate (d) corresponds to the fault distance computed for the other healthy phase. Based on the initial estimate of distance(d), we use equation 3.7 to compute the load current in the faulted phase considering phase c as the faulted phase.

$$\begin{aligned}
 V_c &= V_{fc} + d \times (I_a \times Z_{ca} + I_b \times Z_{cb} + I_c z \times Z_{cc}) \\
 V_{fc} &= (1 - d) \times (I_a \times Z_{ca} + I_b \times Z_{cb} + I_{loadc} \times Z_{cc}) + I_{loadc} \times Z_{loadc}
 \end{aligned} \tag{3.7}$$

where V_{fc} is the voltage at the fault point, Z_{loadc} is the impedance of the load in phase C and I_{loadc} is the phase c post-fault load current. A modification of equation 3.6, which incorporates change in load current, is depicted in equation 3.8.

$$\begin{aligned}
 V_a - V_{a_{\text{prefault}}} &= (I_a - I_{a_{\text{prefault}}}) \cdot (Z_{aa} + Z_{load_a}) \\
 &+ (I_b - I_{b_{\text{prefault}}}) \cdot Z_{ab} + (I_c - I_{c_{\text{prefault}}}) \cdot d \cdot Z_{ac} + (I_{loadc} - I_{c_{\text{prefault}}}) \cdot (1 - d) \cdot Z_{ac}
 \end{aligned} \tag{3.8}$$

$$\begin{aligned}
 V_b - V_{b_{\text{prefault}}} &= (I_b - I_{b_{\text{prefault}}}) \cdot (Z_{bb} + Z_{load_b}) \\
 &+ (I_a - I_{a_{\text{prefault}}}) \cdot Z_{ba} + (I_c - I_{c_{\text{prefault}}}) \cdot d \cdot Z_{bc} + (I_{loadc} - I_{c_{\text{prefault}}}) \cdot (1 - d) \cdot Z_{bc}
 \end{aligned}$$

Equation 3.8 is used for calculating the fault distance (d) incorporating the change in the load current in the faulted phase.

3.3.2 A single lateral case

Consider a system as shown in figure 3.5 with two PMUs at two ends of a trunk and a single lateral branch connected between these PMUs. The lateral branch has a load connected at its end. All the line parameters are known. We use third harmonic measurements from two PMUs to find the distance to the fault in the main trunk. If the obtained distance to the fault is near to the lateral branch, we use a proposed single ended fault location algorithm to find the distance to the fault in the lateral. The voltage at the point where the lateral is connected can be obtained using accurate distribution system model given by equations 2.12 and 2.13.

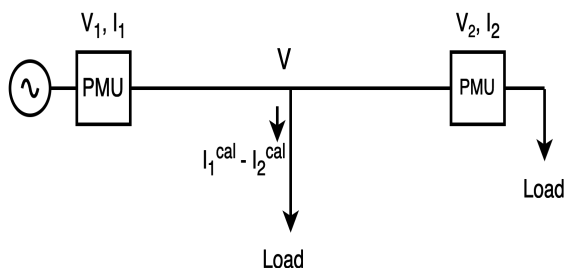


Figure 3.5: System with a single lateral

The voltage at the lateral can be obtained from both PMU1 and PMU2 in this case. These values are very close to each other and we can take their average. The current flowing to the lateral is calculated using KCL given in equation 3.9

$$I_{lateral} = I_1^{cal} - I_2^{cal} \quad (3.9)$$

where I_1^{cal} and I_2^{cal} are calculated using equations 2.12 and 2.13. The percentage accuracy

of the fault is calculated as:

$$\%Error = \frac{|\text{Actual fault location} - \text{Estimated fault location}|}{\text{Total line length}} \times 100 \quad (3.10)$$

3.3.3 Two lateral case

Consider a system as shown in 3.6 where two PMUs are installed at the two ends of a trunk and there are two laterals between them. Each lateral has load connected at its end. The

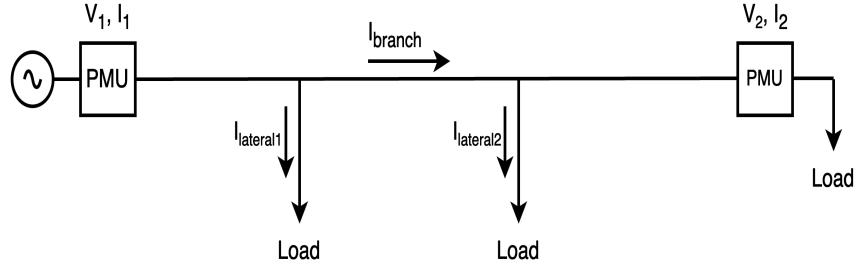


Figure 3.6: System with two laterals

current that is flowing between two laterals is given by:

$$I_{branch} = \frac{V_{lateral1} - V_{lateral2}}{Z_{branch}} \quad (3.11)$$

where, $[V_{abc}]_{lateral1}$ is the voltage at the 1st lateral calculated using equation 2.13. And, $[V_{abc}]_{lateral2}$ is the voltage at the 2nd lateral calculated using equation 2.12 The current flowing in the 1st lateral is given as:

$$I_{lateral1} = I_1^{cal} - I_{branch} - \frac{Y_{abc}}{2} \times V_{lateral1} \quad (3.12)$$

where I_1^{cal} is obtained using equation 2.13.

Similarly, the current flowing in the 2^{nd} lateral is calculated as:

$$I_{\text{lateral2}} = I_{\text{branch}} - \frac{Y_{\text{abc}}}{2} \times V_{\text{lateral2}} - I_2^{\text{cal}} \quad (3.13)$$

where I_2^{cal} is obtained using equation 2.12.

In both single-ended and two-ended methods, the phasors at the node where lateral is connected are accurate. Thus, it is expected that the fault distance would be accurate. There can be a minor error in the fault distance estimation as the effect of shunt capacitance is not included in the fault distance equation and some minor error from phasor computation. In the case of three phase system, with a single line to ground fault, the errors in the distance calculation would be almost same, and some difference is due to the fact that the system is unbalanced and the current flowing in different phases is different and thus capacitive current is different.

Chapter 4

Result

This section presents the main results obtained using the fault location methodology explained in Chapter 3. For the location of the fault in lateral branches, ATP-EMTP and Matlab software is used for the simulation and the validation of different methodologies as is the case in existing literature [12], [13]. As the voltages and currents signals obtained using EMTP software are represented in time domain, the DFT algorithm described in Chapter 2 was used for estimating the phasors.

4.1 A single lateral Case

A HIF is applied along the length of a line to the system with a single lateral described in 3.5. The total length of the line is 3.048 km and is modeled through π circuits. The system has a radial configuration and the voltage at the substation is 4.16 KV. A HIF with resistance of 100 ohms was selected to limit the fault current to under 20% of the total current measured by PMU at the substation. Similarly, the value of V_P and V_N are 900 V and 950 V respectively for maintaining the required percentage of third harmonic in the fault current as mentioned in [10] and the asymmetry of HIF. Initially, the distance to the fault is calculated by applying two-ended impedance based method. Table 4.1 represents both the actual and calculated distance to the fault from the PMU at the substation. From the table, we can observe that in each case, the algorithm provides a fault distance very close to the actual

Expected Fault Distance (m)	Calculated Fault Distance (m)
304.8	292.6
1219.2	1208.22
2438.4	2435.96
3048	3049.83

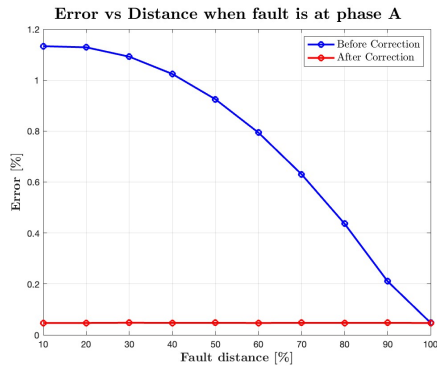
Table 4.1: Comparison of Expected and Calculated Fault Distances

distance. However, there is a small error attributed to spectral leakage from the lateral. If the distance to the fault calculated using two ended FLA is close to any lateral, a single ended fault location algorithm is run to verify if the fault has occurred in the lateral and calculate the fault distance in the lateral branch.

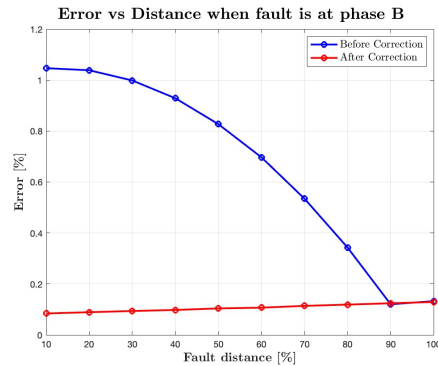
Case: When a fault is applied at different phases and along the line in a lateral branch:

For these cases, results of before correction corresponds to the result when the current downstream of the fault point is taken as constant and results after correction corresponds to results when the change in that current is incorporated in the calculation of fault distance. The fault distance is computed using equation 3.6 and 3.8 for before and after correction cases respectively. The error in the distance calculation is computed using equation 3.10. Figures 4.1a, 4.1b, 4.1c, represents the error in the distance calculated as a function of the fault distance for different phases.

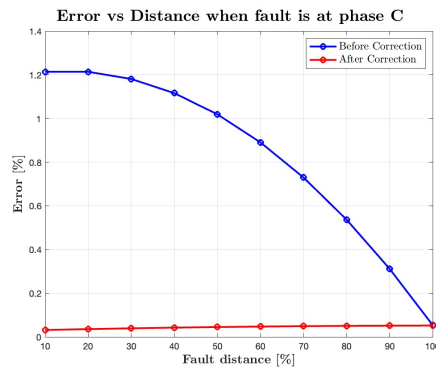
During a HIF, there is a small change in the voltage at a fault point. A good initial estimate of the fault current I_f would be to assume it to be equal to the difference between post-fault and pre-fault current which make the load current constant in the first iteration [12]. However, this small change in the voltage also leads to a small change in the load



(a) Fault at Phase A



(b) Fault at Phase B



(c) Fault at Phase C

Figure 4.1: Faults at different phases

current in the faulted phase. From figures 4.1a, 4.1b, 4.1c, it becomes evident that incorporating the change in this current in the fault distance calculation reduces the calculated error in the fault distance estimation. This makes sense because the part of a distribution line downstream from the fault point, also has mutual impedance associated with it which has an effect on the voltage of a healthy phase. Even though the change in the load current is small, it has some contribution. Ignoring this current leads to an error in the estimation of fault distance. Similarly, we observe a reduction in percentage error as the fault distance increases in before correction cases. This phenomenon occurs because with an increasing fault distance, the percentage of the line and therefore the impedance downstream from the fault point decreases. Consequently, the influence of the mutual impedance, which has

not been accounted for in the voltage change of the healthy phase, also decreases. When a fault occurs at the end of a lateral line, precisely at 100% of its length, the calculated fault distance before and after correction is same. This is due to the fact that in such cases, the effect of mutual impedance of the entire line is already incorporated in the equation before correction. In the cases after correction, we can observe that there is a very small error in the fault distance estimation. The error in the distance estimation is almost constant with the variation of fault distance along the line. One of the contributing factors to this error is the neglect of the capacitive effect of a line. For all cases, the error is within 0.13%.

4.2 Two lateral Case

A system with two laterals, as described in Figure 3.6, and operating at 4.16 kV, is modeled for this case. The total length of the line is 4.572 km, divided into three sections of 1.524 km each, modeled with π circuits. The length of both lateral lines is 2.4384 km. HIFs are simulated along the line, lateral branches, and in different phases. The fault has a steady-state value of 100 ohms, and the values of V_P and V_N are 900V and 950V, respectively. Initially, a two-ended method using third harmonic voltage and currents measured by two PMUs is applied to calculate the distance to the fault. Table 4.2 represents both the actual and calculated distance to the fault from the PMU at the substation . From the table, we can see

Expected Fault Distance (m)	Calculated Fault Distance (m)
457.2	412.39
1524	1485.9
2743.2	2732.22
3657.6	3671.3
4572	4609.03

Table 4.2: Comparison of Expected and Calculated Fault Distances

that the calculated fault distance is very close to the actual distance to the fault. Also, the error is higher compared to single lateral system, as there are two laterals in this system and this leads to a higher leakage current. A single ended method is applied in the case when the fault distance calculated using the two ended method is near the lateral branch. The fault is placed at intervals of 10%, from 10% to 100% along the lateral branch. Figure 4.2 represents graphs of the error as a function of the fault distance when the single ended FLA is applied.

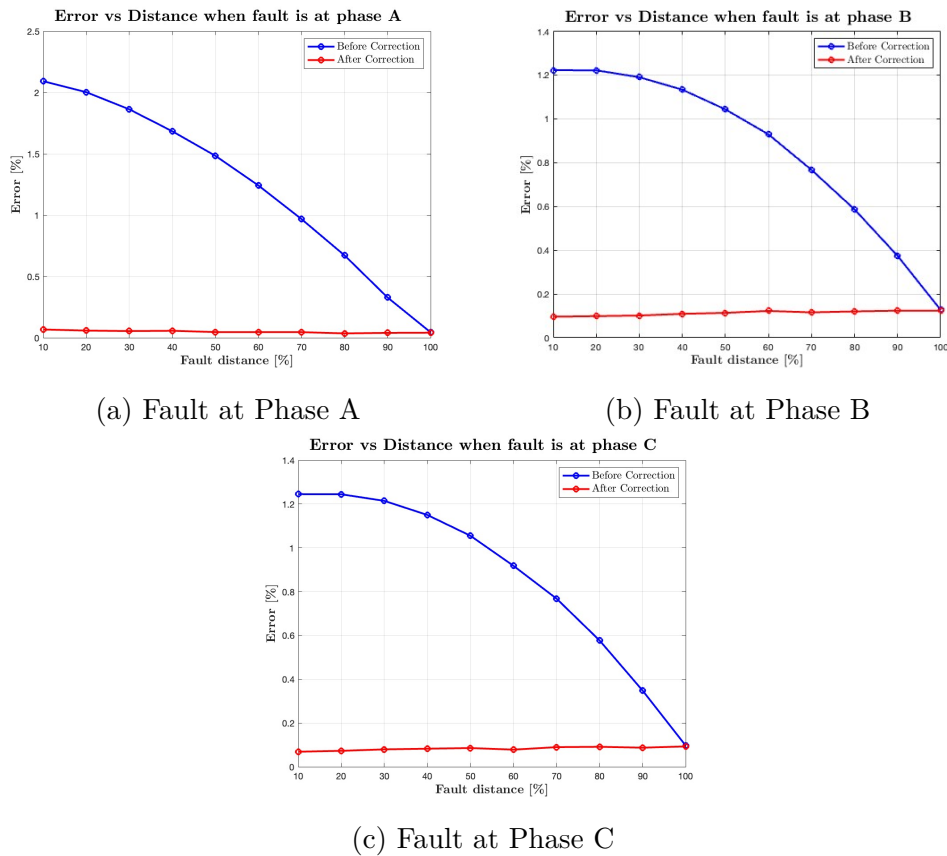


Figure 4.2: Faults at different phases

The minor error in the fault distance calculation in after correction case is the result of ignoring capacitor current. The single ended FLA has a small error which is verified from

simulations and thus it confirms that the fault is in the lateral branch. The trend in the error percentage with respect to the distance to the fault is similar to a single lateral system with error less than 0.2%. The analysis explained for the percentage error for faults in single lateral system is valid for this system as well.

4.3 Six Bus System

Consider a six-bus system shown in Figure 4.3 with a main feeder and six lateral branches with different lengths. The voltage at the substation is 13.8 KV. All the single-phase lateral branches have been modified to two phases. There are six nodes with node 1 being the substation node, and subsequent nodes numbered sequentially. The system has a radial configuration. Three PMUs are placed along the main feeder. In [15], by placing two PMUs

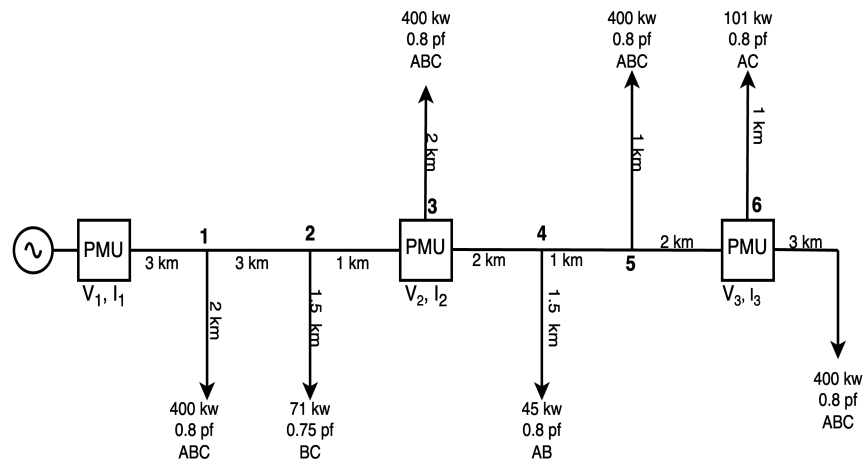


Figure 4.3: Six Bus System [15]

at the two ends of a main feeder, the author was able to measure the distance to the fault in the main feeder. However, the laterals were a blind spot to their algorithm. Placing PMUs in the described configuration and using algorithms described in chapter 3, we are able to measure the distance to the fault when the fault occurs either in a trunk or in a lateral

branch. A HIF with a steady-state resistance value of 500 ohms, and V_P and V_N values of 5000 V and 5500 V, respectively, is applied to the system. Fault is placed along the main feeder and the laterals and the two-ended FLA is applied to compute the distance to the fault from substation. The percentage errors in the fault distance estimation are shown in Table 4.3.

Distance to the fault from Substation (Km)	Computed Percentage Error
3	2.29
5	2.218
6	2.20428
7	2.22
9	0.43
10	0.25
11	0.09
12	0.41

Table 4.3: Percentage error in fault distance calculation using two-ended FLA

PMU 1 is placed at the substation node, PMU 2 at 7 km from the substation and PMU 3 at 12 km from substation. In cases where a fault occurs between PMU 1 and PMU 2, the error is higher, as shown in Table 4.3. This higher error can be attributed to the fact that the distance between these PMUs is larger compared to the distance between PMU 2 and PMU 3. Additionally, in the lateral branches between these PMUs, the load has relatively lower impedance, allowing for higher leakage current. Thus, the load impedance in the lateral branches affects the accuracy of fault location when two-ended FLA is used. In scenarios where the fault occurs downstream from PMU 3, the fault distance computed using these PMUs exceeds the total line length. Thus, we can verify that the fault is not in the line between the PMUs. To accurately determine the distance to the fault downstream of PMU 3, a single-ended FLA is employed. Table 4.4 presents the results obtained using the single-ended fault location algorithm when HIF is applied at a certain distance in different laterals. The percentage error is calculated from the distance calculated including the change in the

current downstream of the fault point and is given in Table 4.4.

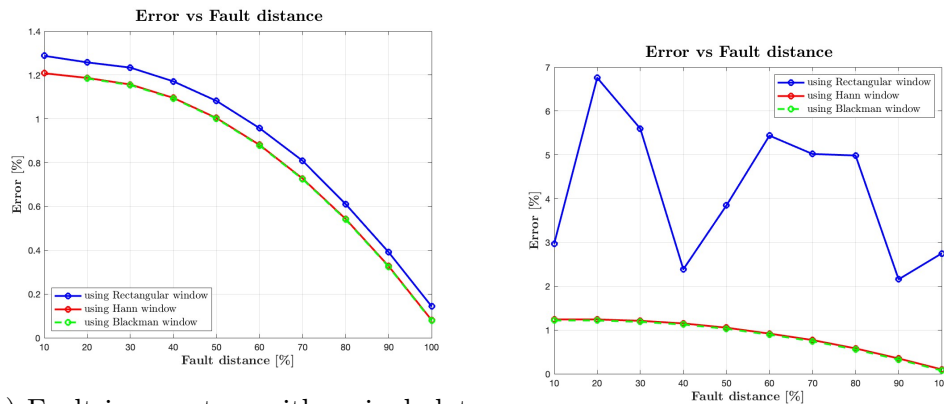
Fault Position	Fault Distance(of the lateral)	Percentage Error
Node 6 towards 400 kw load	2/3	0.23785
Node 6 towards 400 kw load	1/6	0.2658
Node 6 towards 101 kw load	1/2	0.6329
Lateral 5	1/2	0.05565
Lateral 5	1/200	0.53
lateral 1	1/4	0.13955
lateral 3	3/5	0.1652
lateral 2	1/3	0.8688

Table 4.4: Calculated distance to the fault using single-ended FLA

From the table , we can see that in all of cases, the percentage error is lower than 1%. The analysis done for a single lateral case also applies here. A single-ended impedance-based fault location algorithm encounters multiple estimation problems in the presence of two branches, and this scenario arises at node 6 if a two-ended FLA is not used. For instance, consider a case where a fault occurs at the middle of a lateral connected to a 101 kW load at node 6. If we treat this particular lateral as the faulted lateral and calculate the distance to the fault, we obtain the correct fault distance. However, if we assume the fault occurs at the line section downstream from PMU 3 and calculate the fault impedance, we find the fault to be at 92.49% of that line. This results in multiple estimations of the fault location, which increases the overall recovery time. Running a two-ended FLA before a single-ended FLA allows us to verify that the fault lies at the end of a line connected between PMU 2 and PMU 3, i.e. at node 6. Thus, we can confirm the correct faulted lateral.

4.4 Comparison of different windows for phasor computation

The Voltage and current signals generated by EMTP-ATP are in time domain. The pre-fault and post-fault samples are multiplied with the factors of different windowing functions and their fourier transform is computed. The rectangular, Hann and Blackmann windows have been compared as they are the most common windows used in PMUs[20]. Figure 4.4 represents the error as a function of the fault distance when different windows are used. From the figure, we can see that the error is higher for rectangular window compared to



(a) Fault in a system with a single lateral

(b) Fault in a system with two laterals

Figure 4.4: Fault at phase A in 2nd lateral

Hann and Blackmann windows, in all of the cases. This is due to the spectral leakage phenomenon described in section 2.2. As a result, the voltage and current phasors are slightly less accurate. When the fault distance is calculated using these phasors, there will be higher deviation from the expected distance and thus the error percentage will be higher. In the system with two laterals, the error is considerably higher when rectangular window is used compared to other two windows. This increase in error can be attributed to the estimation of voltage and current at nearby nodes using less accurate phasors and error goes

on accumulating. Higher error has been observed in the estimation of I_{branch} in equation 3.11. Thus, when the system has prominent harmonic component in a signal, it is advisable to use a PMU that uses a windowing function with smaller spectral leakage according to the desired application. In this thesis work, Hann window has been used for every cases as the errors calculated using both Hann and Blackmann window are almost same and the central lobe for Blackmann window is wider than that of Hann window.

4.5 Sensitivity Analysis

4.5.1 Sensitivity to noise

A gaussian noise of SNR 45 db is added to the signals measured using EMTP-ATP software. The DFT is performed using Hann window. Due to the addition of noise, there is some inaccuracy in both the magnitudes and angles of the fundamental phasors. In HIF, there is a small change in the current in the faulted phase, and thus smaller change in the voltage in a healthy phase. The change in the voltage and current for different distance is close to each other and thus even the small error in the phasors of voltages and current leads to an error in the distance estimation. Fig 4.5 presents the percentage errors as a function of distance without noise and with 45 db noise in the measurements. We can see in figure 4.5 that the algorithm is sensitive to the noise as the addition of noise has increased the error in the estimation of the distance to the fault.

4.5.2 Sensitivity to load

Simulations were performed for all systems for different loading conditions. The HIF was applied along the lateral branch and the fault distance was computed for each case. Figure

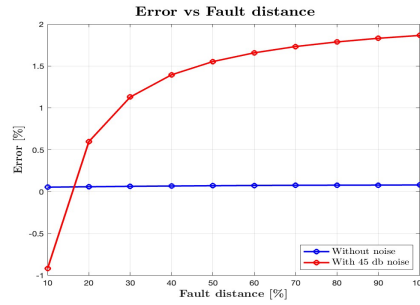


Figure 4.5: Estimated distance percentage error as a function of distance considering noise in the measurement

4.6 represents the percentage error in the calculation of fault distance under different load conditions for a system with two laterals. L1, L2, and L3 represents varying levels of load: light, moderate, and heavy, respectively. The graph has some random characteristics but the error percentage is still very close to each other. It proves that the algorithm is not significantly sensitive to the load variations in a system. Thus, it is suitable in all systems regardless of their loads.

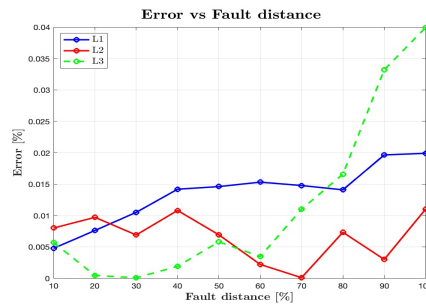


Figure 4.6: Estimated distance percentage error as a function of distance under different load conditions

Chapter 5

Conclusions and Future Work

The objective of this thesis work was to develop a single ended fault location algorithm for HIF that is able to find the distance to the fault in the lateral branch of a distribution system. This was successfully achieved.

A model is developed that represents the physical characteristics of a HIF. A two ended impedance-based method is implemented to find the distance to the fault in the main trunk. For HIFs in lateral branches, a single ended FLA is required. Due to the non-linear nature of the HIF, computing the fault distance using the measurement of a faulted phase results in an underdetermined equation. During the fault, there is a change in the current in the faulted phase which results in a change in the voltage of healthy phases. An equation is developed that relates the fault distance with the change in the voltage of a healthy phase. While the focus is primarily on single-phase-to-ground HIF, the algorithm works effectively for rare but possible double line-to-ground HIFs as well. Extensive testing across diverse systems validates the reliability and accuracy of the algorithm. However, a notable limitation of this algorithm is that it requires at least one healthy phase running parallel to the faulty phase. The phasors have been computed using Hann window because of the spectral leakage phenomenon associated with a rectangular window. The algorithm has been tested for different loading conditions and 45 db noise in the system. The algorithm has a non-significant sensitivity to the loading conditions, however is sensitive to the noise.

For the future work, we can look into improving the accuracy of the algorithm in the presence of noise. Similarly, accurate calculation of load impedance requires limiting lateral branches between two PMUs to two. One can look into methods to estimate load impedance accurately even with multiple laterals, reducing the number of required PMUs in the system for the calculation of the fault distance.

Bibliography

- [1] A. Bahmanyar, S. Jamali, A. Estebarsari, and E. Bompard, “A comparison framework for distribution system outage and fault location methods,” *Electric Power Systems Research*, vol. 145, pp. 19–34, 2017.
- [2] A. Ghaderi, H. A. Mohammadpour, H. L. Ginn, and Y.-J. Shin, “High-impedance fault detection in the distribution network using the time-frequency-based algorithm,” *IEEE Transactions on Power Delivery*, vol. 30, no. 3, pp. 1260–1268, 2015. doi: [10.1109/TPWRD.2014.2361207](https://doi.org/10.1109/TPWRD.2014.2361207).
- [3] S. Hossain, H. Zhu, and T. Overbye, “Distribution high impedance fault location using localized voltage magnitude measurements,” in *2014 North American Power Symposium (NAPS)*, IEEE, 2014, pp. 1–6.
- [4] G. N. Lopes, T. S. Menezes, D. P. Gomes, and J. C. M. Vieira, “High impedance fault location methods: Review and harmonic selection-based analysis,” *IEEE Open Access Journal of Power and Energy*, 2023.
- [5] S. H. Mortazavi, Z. Moravej, and S. M. Shahrtash, “A searching based method for locating high impedance arcing fault in distribution networks,” *IEEE Transactions on Power Delivery*, vol. 34, no. 2, pp. 438–447, 2018.
- [6] D. P. Gomes and C. Ozansoy, “High-impedance faults in power distribution systems: A narrative of the field’s developments,” *ISA transactions*, vol. 118, pp. 15–34, 2021.
- [7] É. M. Lima, N. S. D. Brito, and B. A. de Souza, “High impedance fault detection based on stockwell transform and third harmonic current phase angle,” *Electric Power Systems Research*, vol. 175, p. 105 931, 2019.

- [8] G. N. Lopes, V. A. Lacerda, J. C. M. Vieira, and D. V. Coury, “Analysis of signal processing techniques for high impedance fault detection in distribution systems,” *IEEE Transactions on Power Delivery*, vol. 36, no. 6, pp. 3438–3447, 2020.
- [9] L. U. Iurinic, A. R. Herrera-Orozco, R. G. Ferraz, and A. S. Bretas, “Distribution systems high-impedance fault location: A parameter estimation approach,” *IEEE Transactions on Power Delivery*, vol. 31, no. 4, pp. 1806–1814, 2015.
- [10] A. Emanuel, D. Cyganski, J. Orr, S. Shiller, and E. Gulachenski, “High impedance fault arcing on sandy soil in 15 kv distribution feeders: Contributions to the evaluation of the low frequency spectrum,” *IEEE Transactions on Power Delivery*, vol. 5, no. 2, pp. 676–686, 1990.
- [11] A. G. Phadke and J. S. Thorp, *Computer relaying for power systems*. John Wiley & Sons, 2009.
- [12] M. J. Ramos, A. S. Bretas, D. P. Bernardon, and L. L. Pfitscher, “Distribution networks hif location: A frequency domain system model and wls parameter estimation approach,” *Electric power systems research*, vol. 146, pp. 170–176, 2017.
- [13] J. Nunes, A. S. Bretas, N. G. Bretas, A. Herrera-Orozco, and L. Iurinic, “Distribution systems high impedance fault location: A spectral domain model considering parametric error processing,” *International Journal of Electrical Power & Energy Systems*, vol. 109, pp. 227–241, 2019.
- [14] J. Doria-Garcia, C. Orozco-Henao, L. Iurinic, and J. D. Pulgarín-Rivera, “High impedance fault location: Generalized extension for ground faults,” *International Journal of Electrical Power & Energy Systems*, vol. 114, p. 105387, 2020.

- [15] D. R. R. Penido, L. R. de Araujo, V. T. Rodrigues, and K. B. do Nascimento, “An analytical zero sequence method to locate fault in distribution systems rich in dg,” *IEEE Transactions on Smart Grid*, vol. 13, no. 3, pp. 1849–1859, 2022.
- [16] J. J. G. Ledesma, K. B. do Nascimento, L. R. de Araujo, and D. R. R. Penido, “A two-level ann-based method using synchronized measurements to locate high-impedance fault in distribution systems,” *Electric Power Systems Research*, vol. 188, p. 106 576, 2020.
- [17] A. G. Phadke and J. S. Thorp, *Synchronized phasor measurements and their applications*. Springer, 2008, vol. 1.
- [18] F. Zhang, Z. Geng, and W. Yuan, “The algorithm of interpolating windowed fft for harmonic analysis of electric power system,” *IEEE transactions on power delivery*, vol. 16, no. 2, pp. 160–164, 2001.
- [19] D.-J. Jwo, I.-H. Wu, and Y. Chang, “Windowing design and performance assessment for mitigation of spectrum leakage,” in *E3S Web of Conferences*, EDP Sciences, vol. 94, 2019, p. 03 001.
- [20] Arbiter Systems, Inc., *Model 1133A Phasor Measurement Specifications*. [Online]. Available: https://www.arbiter.com/files/product-attachments/1133_phasor_measurement_specifications.pdf.
- [21] W. H. Kersting, “Distribution system modeling and analysis,” in *Electric power generation, transmission, and distribution*, CRC press, 2018, pp. 26–1.
- [22] D. Jeerings and J. Linders, “Ground resistance-revisited,” *IEEE Transactions on Power Delivery*, vol. 4, no. 2, pp. 949–956, 1989.

- [23] W. C. dos Santos, B. A. de Souza, N. S. D. Brito, F. B. Costa, and M. R. C. Paes, “High impedance faults: From field tests to modeling,” *Journal of Control, Automation and Electrical Systems*, vol. 24, pp. 885–896, 2013.
- [24] S. Nam, J. Park, Y. Kang, and T. Kim, “A modeling method of a high impedance fault in a distribution system using two series time-varying resistances in emtp,” in *2001 Power Engineering Society Summer Meeting. Conference Proceedings (Cat. No. 01CH37262)*, IEEE, vol. 2, 2001, pp. 1175–1180.
- [25] M. Farajollahi, A. Shahsavari, and H. Mohsenian-Rad, “Location identification of high impedance faults using synchronized harmonic phasors,” in *2017 IEEE Power & Energy Society Innovative Smart Grid Technologies Conference (ISGT)*, IEEE, 2017, pp. 1–5.
- [26] F. Calero, “Mutual impedance in parallel lines—protective relaying and fault location considerations,” in *34th annual western protective relay conference*, 2007, pp. 1–15.
- [27] S. M. Hashemi, M. T. Hagh, and H. Seyedi, “A novel backup distance protection scheme for series-compensated transmission lines,” *IEEE Transactions on Power Delivery*, vol. 29, no. 2, pp. 699–707, 2014. DOI: [10.1109/TPWRD.2013.2272765](https://doi.org/10.1109/TPWRD.2013.2272765).